Electronic Supplementary Material (ESI) for Nanoscale.

Supporting Information

The Controllable Poly-crystalline Bilayer and Multilayer Graphene Film Growth by Reciprocal Chemical Vapor Deposition

Qinke Wu[1], Seong Jun Jung[1], Sungkyu Jang[1], Joohyun Lee[1], Insu Jeon[2], Hwansoo Suh[2], Yong Ho Kim[1,3], Young Hee Lee[4], Sungjoo Lee[1,5,6]* and Young Jae Song[1,4,7]**

Conditions for Reciprocal CVD

a

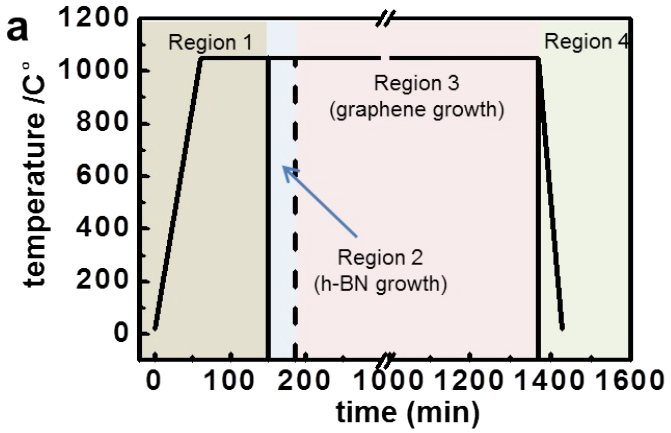

#	Region 1	Region 2	Region 3	Region 4
step	Pre-annealing	h-BN	Graphene	Cooling
H_2	70 sccm	5 sccm	5 sccm	5 sccm
Ar	30 sccm	30 sccm	0 sccm	30 sccm
Etc.	0 sccm N/A	0.5 sccm (borazine+N_2)	0.5 sccm (CH_4)	0 sccm N/A

b

Growth Mode	Graphene/h-BN	Multilayer graphene
H_2	40 sccm	5 sccm
CH_4	40 sccm	0.5 sccm
growth time	40 min (2 nm thick) 60 min (5 nm thick)	12 hours

Figure S1. Conditions used for graphene growth. (a) Temperature profile and flow parameters during the growth of epitaxial multilayer or poly-crystalline bilayer graphene. (b) Table listing the growth conditions used to prepare the graphene/h-BN heterostructure and the multilayer graphene.

Control of h-BN Thickness by Controlling the Growth Time

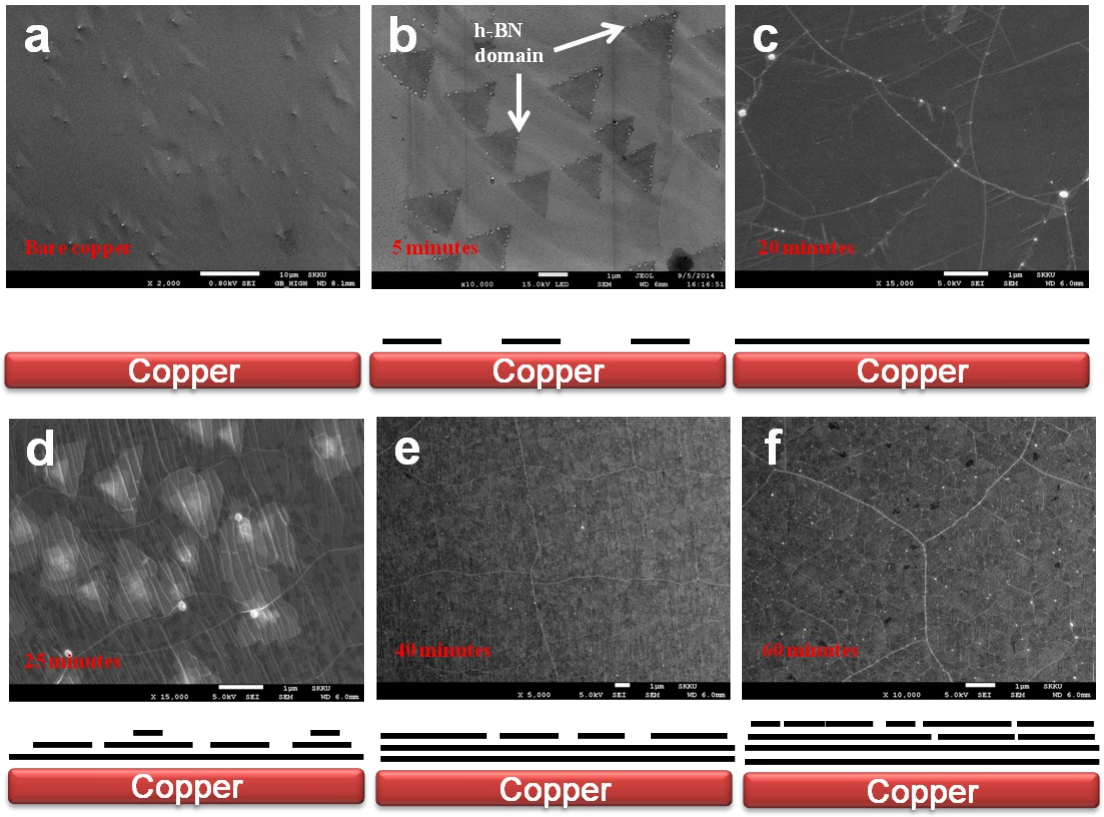

Figure S2. (a) is the SEM image of bare copper surface; (b) is the SEM image of h-BN domains on copper after 5 minutes growth; (c) is the SEM image of fully h-BN monolayer film on copper after 20 minutes growth; (d) is the SEM image of some h-BN ad-layers on the first-grown layer, after 25 minutes growth; (e) and (f) are the SEM images of h-BN film with many layers after 40 and 60 minutes growth, respectively;

Thickness of a h-BN Film (40 min growth, Measured on SiO_2)

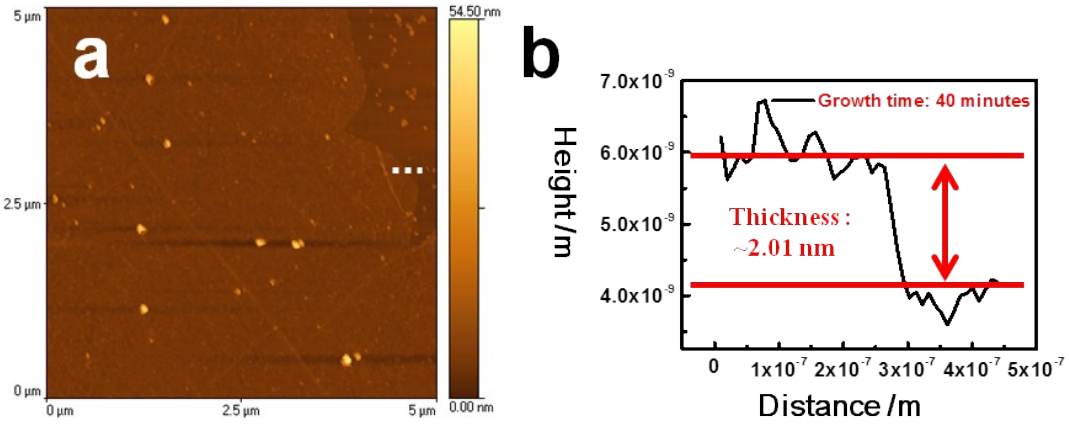

Figure S3. (a) is the AFM image of the 40 minutes grown h-BN, after transferring onto SiO_2 substrate; (b) is the line profile along the dashed white line in (a), which shows the thickness of the h-BN is around 2 nm.

Uniformity of h-BN Films

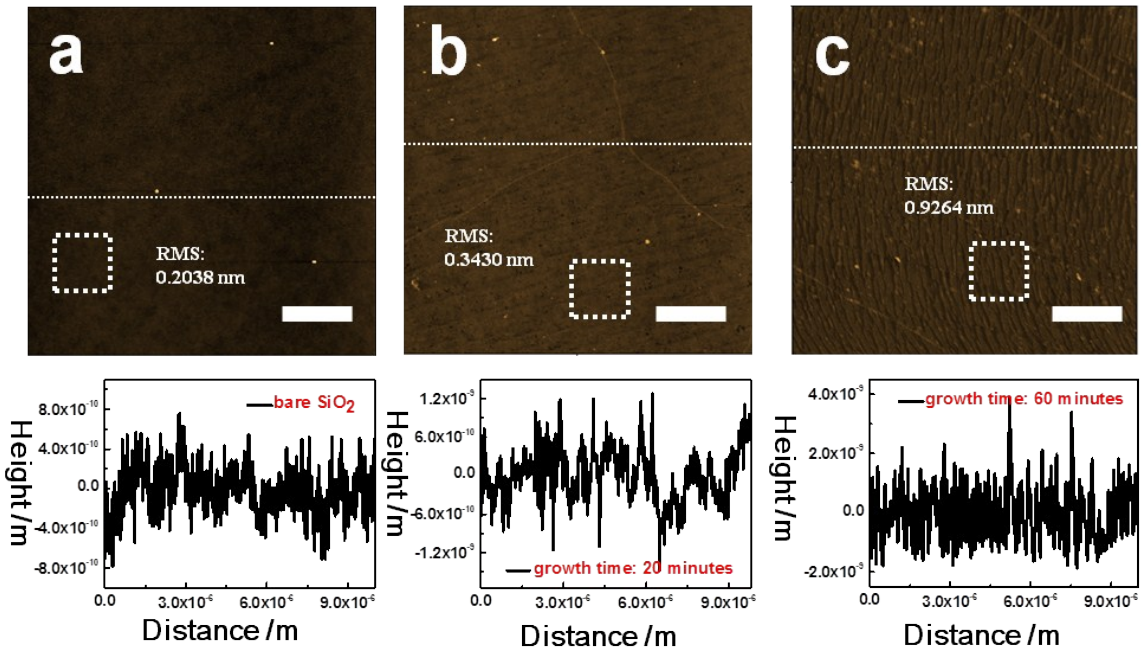

Figure S4. (a) is the AFM image of the bare SiO_2 substrate; (b) and (c) are the AFM image of monolayer and 60 minutes (~5 nm thick) grown h-BN after transferring onto SiO_2 substrate. From the RMS of (c), we can see that its surface is still very uniform comparing with monolayer h-BN in (b). All the scale bares are 2 μm.

Graphene Growth without h-BN to Compare Normal and Reciprocal CVD.

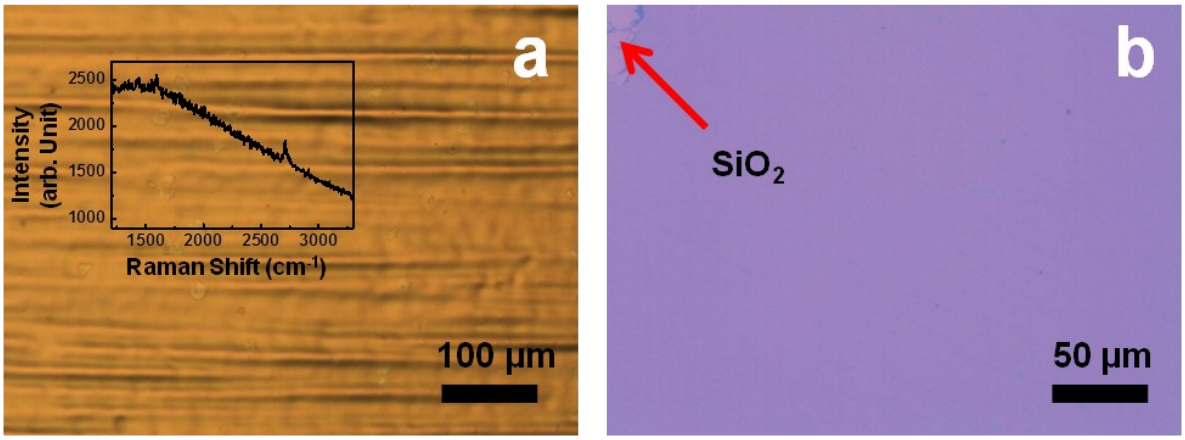

Figure S5. (a) is the OM image of graphene grown on a bare copper foil, under the same growth conditions of Figure 1b and 1c; the inset Raman spectra shows that it is monolayer graphene; (b) is the OM image of the graphene grown in (a) and it shows uniform color contrast of monolayer, after transferring onto SiO_2 substrate.

Intra-/Inter-island Angle Distribution in the Multilayer Graphene: The topologies of the multilayer graphene grown using a 2 nm thick h-BN film were statistically analyzed because

the graphene islands grown using a 5 nm thick h-BN film were too small to measure the exact edge angles between graphene layers. Figures S6(a)–S6(h) show a series of OM images of multilayer graphene islands having 2–9 layers. Most graphene islands were hexagonal with parallel edges in each layer, with a maximum layer size of 120 μm for the bilayer, 56 μm for the trilayer, 28 μm for the four-layer, 29 μm for the five-layer, 22.2 μm for the six-layer, 18 μm for the seven-layer, and 10 μm for the eight-layer films. Figure S6(i) shows a histogram of the edge angles obtained from the various graphene layers in a given graphene island (intra-island angles). The angles were perfectly parallel between the 3rd and higher-index layers, although the edge angles were incompletely parallel (~93%) between the 2nd and 3rd layers. Figure S7 presents the results of a statistical study of the edge angles of neighboring graphene islands (inter-island angle). The full-area graphene layer on top (the first graphene layer) formed a mother layer that was shared by all graphene islands; therefore, the inter-island angles were measured between neighboring mother bilayers in each multilayer graphene island. Figure S7(c) indicates that 0° and 60° were the preferred angles (62.0%), and a small distribution (11.6%) of inter-island angles occurred at 30° and 85°. The shapes of the graphene islands, as observed in the OM images and intra-/inter-island angle histograms, suggested the epitaxial growth of multilayer graphene, as modeled in Figure S8. Small deviations in the intra-/inter-island angles were observed, as shown in Figures S6–S7, although these were localized to the 1st and 2nd layers and may have been due to the finite domain sizes of the underlying h-BN layer.

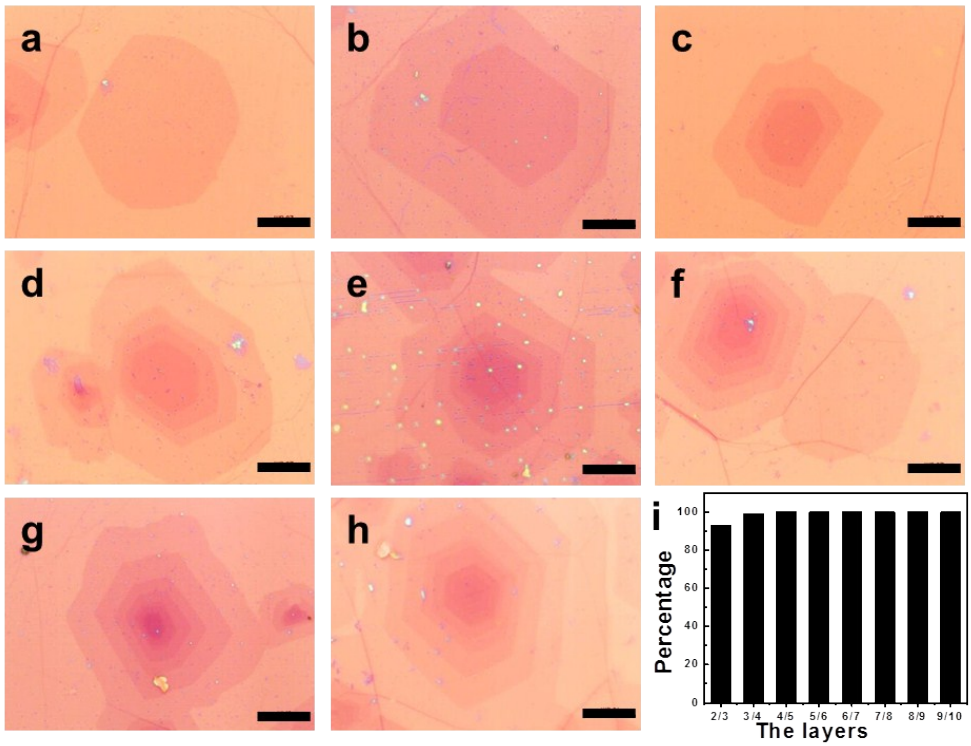

Figure S6. Statistical study of the intra-island angles. (a)–(b) show OM images of multilayer graphene islands having 2–9 layers. (i) Histogram showing the edge angles measured from various layers in a given graphene island. The graphene was grown using a 2 nm thick h-BN film template. The scale bars in (a)–(g) indicate 20 μm, and the scale bar in (h) indicates 10 μm.

Statistical Study of the Inter-island Angles

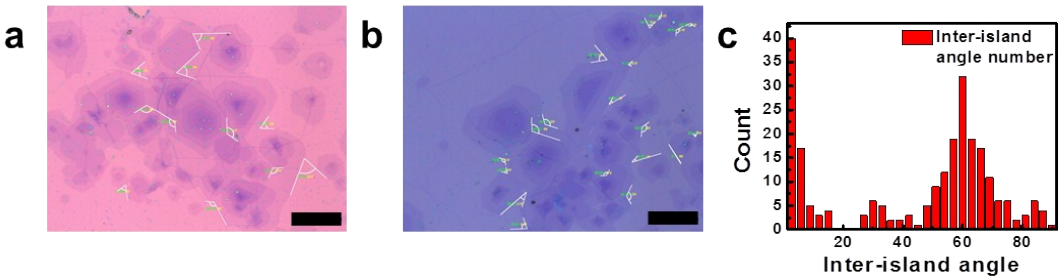

Figure S7. Statistical study of the inter-island angles. (a)–(b) OM images of multilayer graphene islands, at two different positions within a given Cu foil. (c) Histogram of the edge angles measured from the mother bilayers of neighboring graphene islands. Graphene was grown using a 2 nm thick h-BN film template. The scale bars in (a)–(b) indicate 50 μm.

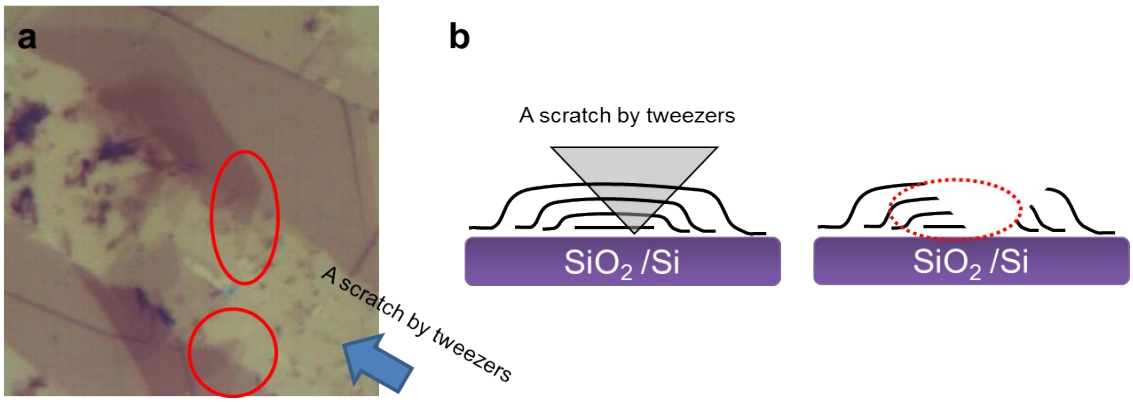

Figure S8. The smaller graphene island was positioned beneath the larger (top) layer. (a) OM image of epitaxial multilayer graphene scratched using tweezers. (b) Schematic diagram showing that the smaller graphene layers (with a greater number of adlayers) survived the tweezers scratch (indicated by the red solid circles in (a) and the red dotted circle in (b)).

Positions of the Adlayers in Multilayer Graphene: AFM measurements could not be used to determine whether the small-area higher-index graphene layers were positioned below or above the first graphene layer. This information was obtained using a simple trick, as illustrated in Figure S8. Tweezers were used to scratch the surface of the multilayer graphene. Although the top layer suffered significant damage by the tweezers, parts of the bottom layers remained protected by the top layer and survived. The OM image (the red circles) shown in Figure S8(a) clearly revealed the surviving pieces of the adlayers (small-area graphene), indicating that the small graphene adlayers were positioned beneath the top graphene layer. These results agreed well with a recently published report.[2]

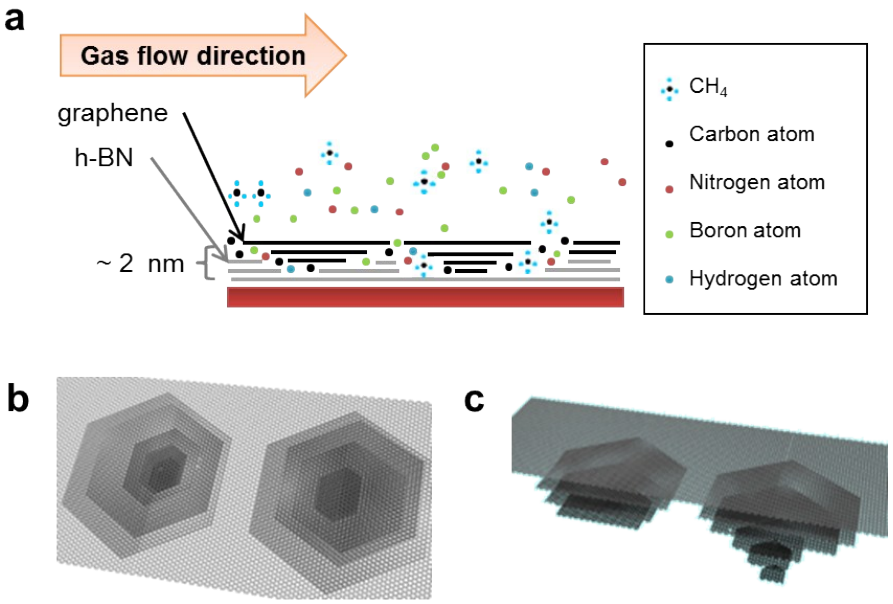

Figure S9. Growth model for the reciprocal CVD process. (a) Schematic diagram illustrating the growth mechanism during the reciprocal CVD process involving simultaneous graphene growth and h-BN etching. (b)–(c) 3D rendered images of epitaxial multilayer graphene islands with bird's eye and cross-sectional views.

Growth Model of Multilayer/Bilayer Graphene in Reciprocal CVD Process: A model of multilayer/bilayer graphene growth during the reciprocal CVD process was proposed, as illustrated in Figure S9. The different growth conditions of the multilayer graphene and graphene/h-BN heterostructures are described in detail in Figure S1. Both structures initially included an h-BN film that had been pre-grown on a Cu foil under given growth conditions, suggesting that the h-BN layer quality and thickness were identical across samples. The graphene growth speed during the growth of the graphene/h-BN heterostructure was fast under a high CH_4 flow rate (40 sccm). The underlying h-BN layer was covered and protected quickly (within 40 minutes). Multilayer graphene growth, however, used a very small CH_4 gas flow (0.5 sccm). The graphene growth speed was very slow (12 hours), which exposed the h-BN to residual hydrogen atoms present in the H_2 gas flow or produced by the decomposition of CH_4 at longer times. Although graphene grew on the h-BN film, defect regions in the h-BN layer that had seeded graphene nucleation were preferentially etched

away, leaving channels and holes. The carbon precursors (CH_4) diffused through these channels and holes beneath the growing graphene layer. At the same time, hydrogen atoms released from the carbon precursors (CH_4) etched away the h-BN layer in the vicinity of the growing graphene edge, thereby creating a space between the growing graphene layer and the Cu substrate through which carbon precursors were delivered, as illustrated in Figure S9(a) The reciprocal CVD process involving simultaneous graphene growth and h-BN etching stopped when the first graphene layer covered the entire surface area, and multilayer/bilayer graphene was obtained without residual h-BN, as shown in Figures S9(b)–S9(c).

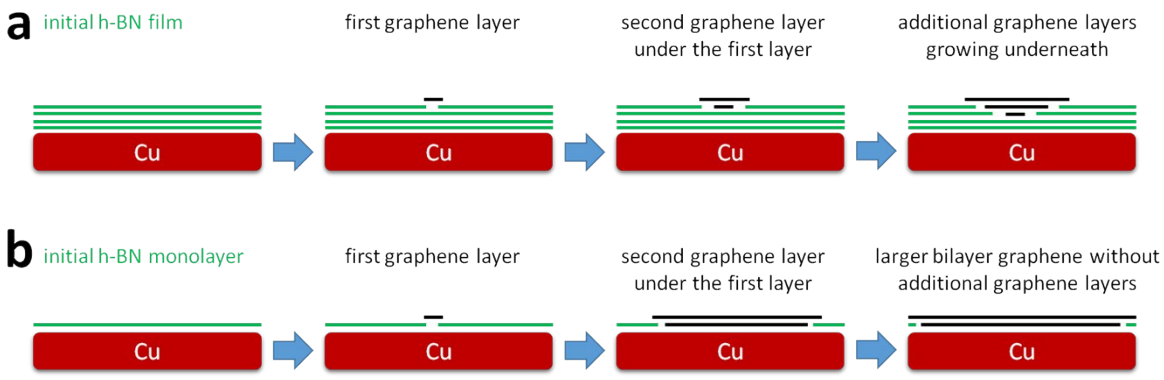

Figure S10. (a) and (b) are the schematic diagram to show the details of the multilayer graphene growth on thick h-BN film/copper and bilayer graphene growth on monolayer h-BN/copper substrates, respectively.

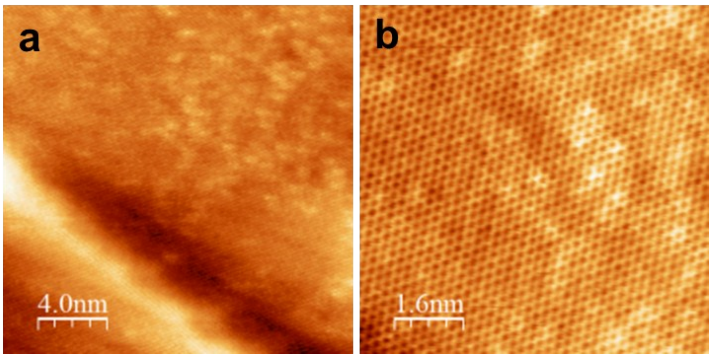

Figure S11. Atomic-resolution scanning tunneling microscopy images of graphene, showing a honeycomb lattice on the top graphene layer.

Crystallinity of the Graphene Layer: Figure S11 shows atomic-resolution scanning tunneling microscopy (STM) images that reveal a honeycomb lattice on the top graphene layer. The images were collected from as-grown epitaxial multilayer graphene grown on a Cu foil prior to transfer to a SiO_2 substrate.

TEM/SAED Measurements Obtained from the Trilayer: High-resolution TEM measurements obtained from the poly-crystalline bilayer graphene revealed the presence of trilayer regions in a few cases. Figures S12(a)–S12(b) and S12(d)–S12(f) show atomic-resolution TEM images collected at two different locations, both of which yielded complicated Moiré patterns. Figures S12(c) and S12(f) show SAED data obtained from the above two locations. The twisted angles in the three layers were apparent.

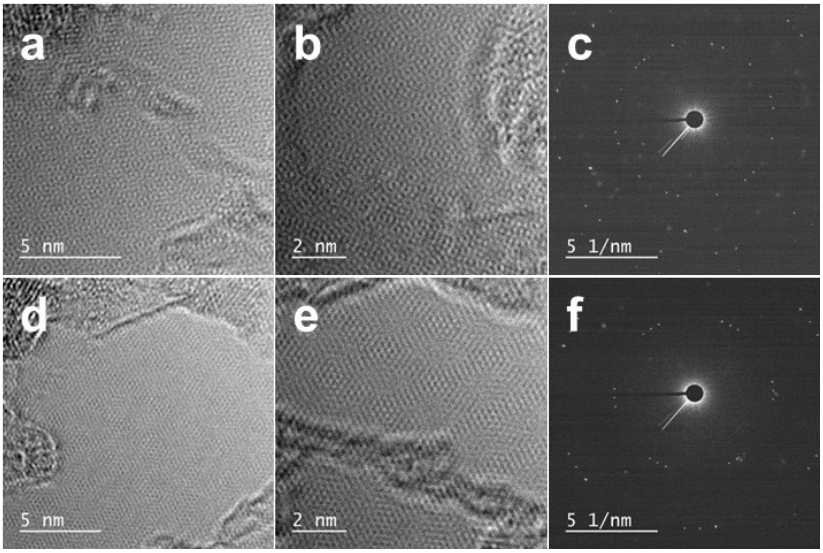

Figure S12. High-resolution TEM images and the corresponding SAED data collected from trilayer regions in a poly-crystalline bilayer graphene sample.

Details in Device Fabrication

The field-effect mobilities were obtained from the transfer curves using the equation:

$$\mu = \left(\frac{L}{WC_{ox}V_D}\right)\left(\frac{\Delta I_D}{\Delta V_G}\right),$$

where L/W are the channel dimensions and C_{ox} is the gate capacitance (38.4 nF/cm^2 for a 90 nm SiO_2 layer).[3] Statistically, bilayer graphene exhibits a lower mobility than monolayer graphene. The difference originates mainly from the effective mass of each material. Monolayer graphene is characterized by a k-linear dispersion in the Brillouin zone, creating an effective mass of zero. Bilayer graphene is characterized by both a k-linear and a k-square dispersion. The effective mass of bilayer graphene is $0.033m_0$, where m_0 is the free-electron mass. [4]

References

[1] M. Wang, S. K. Jang, W.-J. Jang, M. Kim, S.-Y. Park, S.-W. Kim, S.-J. Kahng, J.-Y. Choi, R. S. Ruoff, Y. J. Song, S. Lee, *Adv. Mater.* 2013, *25*, 2746.

[2] Q. Li, H. Chou, J.-H. Zhong, J.-Y. Liu, A. Dolocan, J. Zhang, Y. Zhou, R. S. Ruoff, S. Chen, W. Cai, *Nano Lett.* 2013, *13*, 486.

[3] J.-H. Chen, C. Jang, S. Adam, M. S. Fuhrer, E. D. Williams, M. Ishigami, *Nat. Phys.* 2008, *4*, 377.

[4] E. McCann, *Phys. Rev. B* 2006, *74*, DOI 10.1103/PhysRevB.74.161403.